Available online at www.sciencedirect.com

ScienceDirect

Mendeleev Commun., 2021, **31**, 309–311

Mendeleev Communications

Iron oxide–silver patchy particles prepared by ultrasonic spray burning

Alexey B. Tarasov,[a,b] Ekaterina E. Yurmanova,[a,b] Anna A. Semenova[a] and Evgeny A. Goodilin*[a,b,c]

[a] *Department of Materials Science, M. V. Lomonosov Moscow State University, 119991 Moscow, Russian Federation. E-mail: goodilin@inorg.chem.msu.ru*
[b] *Department of Chemistry, M. V. Lomonosov Moscow State University, 119991 Moscow, Russian Federation*
[c] *N. S. Kurnakov Institute of General and Inorganic Chemistry, Russian Academy of Sciences, 119991 Moscow, Russian Federation*

DOI: 10.1016/j.mencom.2021.05.010

Spray solution combustion synthesis is proposed as a one-step method for preparation of nanostructured iron oxide–silver patchy particles for polyfunctional applications.

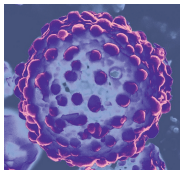

Keywords: patchy particles, silver, superparamagnetic, iron oxide, nanoparticles, surface enhanced Raman spectroscopy, aerosol, combustion.

Patchy particles (PP) form a particular type of microparticles or nanocomposites, the surface or internal volume of which demonstrates polyfunctionality due to the difference in the chemical composition and physical properties of several regions or building blocks combined into one particle.[1,2] The PPs, including the so-called Janus particles[2] as a particular kind with hemispheric patching, have unique properties caused by their asymmetric structure. It consists of different materials connected in a separated manner that ultimately leads to self-assembly or independently controlled surface activity of ensembles of PPs. Silver-containing PPs and nanostructured materials are useful in smart electro-rheological fluids, catalysis, plasmon-induced reactions and surface enhanced Raman spectroscopy for biomedical and environmental applications.[3–12] In this work, spray solution combustion synthesis (SSCS), based on a combination of ultrasonic spray pyrolysis and combustion in a microreactor,[13] was first used to produce† hollow spherical particles composed of plasmonic silver constituents (AgNPs) and superparamagnetic iron oxide nanoparticles (SPION).

The combustion-based approach includes self-sustained chemical reactions in flame synthesis such as gas-phase combustion,[13–15] self-propagating high-temperature heterogeneous synthesis[16,17] and solution combustion synthesis.[18–20] In the latter case, the self-sustained reaction occurs in an aqueous solution of an oxidizing agent such as metal nitrate and fuel, usually glycine. In liquid aerosol flame synthesis,[21] including liquid spray pyrolysis or emulsion combustion, or thermally assisted reactions in aqueous sprays, the initial precursors are in the liquid.[22] The unique feature of these spray-based combustion methods is that they produce particles of an almost spherical shape, which is difficult to achieve with conventional approaches.

Conventional aerosol spray pyrolysis provides pure silver or silver–SPION particles (Figure 1)‡ due to the occurrence of several endothermic reactions that require high temperatures and are controlled mainly by an increase in the system entropy resulting from the formation of a large number of gaseous products [reactions (1) and (2)].

$$2\,[Ag(NH_3)_2OH] = 2\,Ag + 4\,NH_3 + H_2O + 0.5\,O_2 \quad (1)$$

$$2\,Fe(NO_3)_3 = Fe_2O_3 + 6\,NO_2 + 1.5\,O_2 \quad (2)$$

It was previously assumed that ammonia could additionally act as a reducing agent at elevated temperatures, providing a more

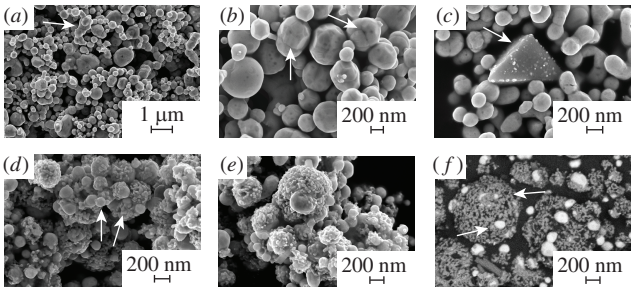

Figure 1 Morphology of (*a*)–(*c*) pure metallic silver microspheres and (*d*)–(*f*) nanocomposites of silver nanoparticles and iron oxides prepared by conventional aerosol spray pyrolysis at 850 °C in air. Note the presence of (*a*),(*b*) multiple junctions of particles, (*b*) facets and (*c*) particles of residual silver(I) oxide indicated by arrows. (*f*) SEM image in BEI mode showing a better contrast between SPION and silver nanoparticles.

† Experimentally, pure silver microspheres were prepared using standard aerosol spray pyrolysis. A stream of ultrasonically generated microdroplets of 0.1 M diamminesilver(I) hydroxide was passed through the hot zone at 850 °C. This silver complex was synthesized from silver nitrate *via* intermediate Ag_2O as reported elsewhere.[8–10] SPION nanocomposites were prepared analogously *via* precipitation of $Fe(OH)_3$ and Ag_2O from a mixture of $Fe(NO_3)_3$ and $AgNO_3$ and subsequent stabilization of silver complex with 5–10 fold excess of aqueous ammonia. In the SSCS method, pure $AgNO_3$, $Fe(NO_3)_3 \cdot 9\,H_2O$ and glycine were used as precursors.[13] The total concentration of spraying solution was 1 M. The Ag^I/Fe^{III} ratio in the solution varied as 1:9, 2:8, 4:6, 6:4, 8:2 and 10:0. The excess of glycine compared to the ideal reaction, $6\,AgNO_3 + 4\,NH_2CH_2COOH \rightarrow 6\,Ag + 8\,CO_2 + 5\,N_2 + 10\,H_2O$, was set as 1.5 or 2. The hot zone temperature was 750 and 850 °C. A flow of air or nitrogen of 1 $dm^3\ min^{-1}$ was used. The resulting PPs were collected with an electrostatic filter. For the formation of initial droplets of *ca.* 0.5–5 μm, an ultrasonic nebulizer with an operating frequency of 2.64 MHz was used.

‡ SEM images here and below were obtained using a Carl Zeiss Leo Supra 50VP scanning electron microscope equipped with an Oxford Instruments INCAEnergy+ EDX/WDX system.

efficient formation of silver nanoparticles[8–10] since the redox potentials of the Ag/Ag^+ and NH_3/N_2 pairs favour the following transformation:

$$3Ag^+ + NH_3 + 3OH^- = 3Ag + 0.5N_2 + 3H_2O. \quad (3)$$

It was also evident that high local heat effects do not drive reactions (1)–(3), and they could proceed through heterogeneous intermediates such as Ag_2O [Figure 1(*c*)], making the final products very chaotic in their microstructure. In particular, these reactions result in a broad particle size distribution, particle junctions, aspherical or disintegrated microspheres [Figures 1(*a*),(*b*)]. The completely different mechanisms of the formation of silver and SPION nanoparticles and, possibly, the interval between the onset of their formation lead to a mixture of AgNPs and SPIONs instead of separate PPs [Figures 1(*d*)–(*f*)].

The SSCS approach is based on strongly exothermic reactions occurring in microreactor droplets of the initial solution and causing combustion:

$$6AgNO_3 + 4NH_2CH_2COOH = 6Ag + 8CO_2 + 5N_2 + 10H_2O, \quad (4)$$

$$2Fe(NO_3)_3 + 10NH_2CH_2COOH + 15O_2 = Fe_2O_3 + 20CO_2 + \\ + 8N_2 + 25H_2O. \quad (5)$$

In this case [reactions (4) and (5)], both the entropy and enthalpy factors make the reaction complete and proceeding much faster. At the same time, it is limited by the geometric boundaries of the initial droplets of the precursor solution. In addition to a higher driving force, combustion produces a higher local temperature, accelerating the separation and crystallization or sintering of the various phase regions in the final microspheres. As a result, PPs are undoubtedly formed [Figures 2(*d*)–(*l*)], which are separated, spherical, hollow, porous, appear to have a narrower size distribution and exhibit a SPION shell or matrix with visible silver patches. Silver and SPIONs are fully separated in these PPs at the nanoscale [Figures 3(*a*),(*b*)],[§] and the assembly of their phases is easy to control macroscopically using the composition of the precursor solution, hot zone temperature and atmosphere. In a nitrogen atmosphere, magnetic PPs are formed since mixed Fe^{II}/Fe^{III} magnetite Fe_3O_4 is observed, while in air, the formation of fully oxidized low magnetic Fe_2O_3 is found [Figures 3(*d*),(*e*)].

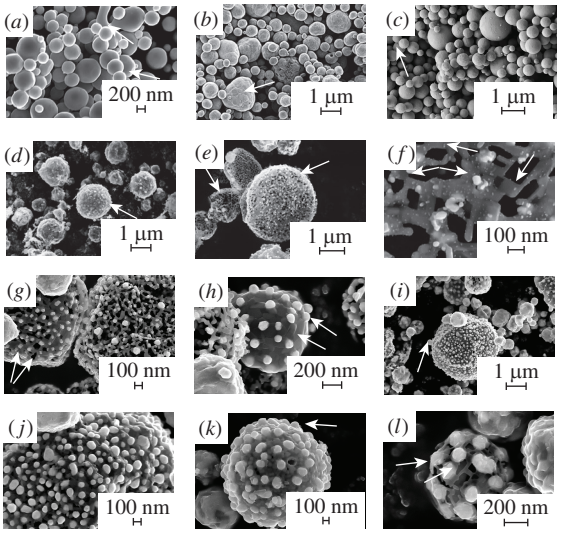

Figure 2 (*a*)–(*c*) Pure isolated silver microspheres and (*d*)–(*l*) PPs with isolated silver patches and SPION matrix prepared by the SSCS method at Ag/Fe ratios of (*d*)–(*f*) 2:8, (*g*),(*h*) 4:6, (*i*)–(*k*) 6:4 and (*l*) 8:2. Arrows indicate (*a*)–(*c*) the facets of silver microspheres and (*f*) two sets of AgNPs and porous crystallized iron oxide on a PP shell. The hot zone temperature was (*a*),(*b*),(*d*)–(*l*) 750 and (*c*) 850 °C. Silver nitrate (oxidizing agent) and glycine were used (*a*) in a stoichiometric ratio [see reactions (4) and (5)], as well as with (*e*),(*f*) a half and (*b*)–(*d*),(*g*)–(*l*) two-fold excess of glycine.

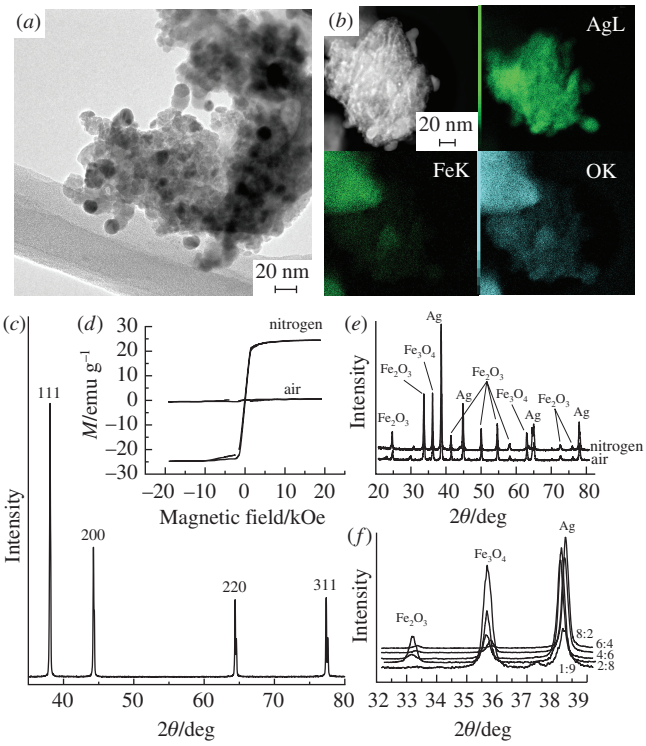

Figure 3 (*a*),(*b*) Nanoscale and (*c*)–(*f*) macroscopic characterization of silver–SPION PPs: (*a*) STEM image, (*b*) X-ray mapping showing the different distribution of silver and iron oxides, (*c*) the phase composition of pure silver microspheres, (*d*) magnetic properties as well as (*e*) X-ray diffraction (XRD) of PPs with Ag/Fe = 2:8 prepared in the air or nitrogen and (*f*) XRD of PPs with a different Ag/Fe ratio (750 °C).

In all cases, mosaic blocks of SPIONs reach 30–50 nm and 25–40 nm for silver, as estimated by the Scherrer formula from XRD data [Figures 3(*c*),(*e*),(*f*)], while observed particles are the same size or 2–3 times larger by SEM/TEM data (see Figures 1–3). The overall size of PPs is in the range of 0.5–3 μm (see Figures 1 and 2), which correlates well with the expected size of droplets produced by the nebulizer since one droplet usually acts as a combustion microreactor.[23,24]

The overall reaction scheme will consist of several main stages, including water evaporation, decomposition of precursors, combustion and silver ions reduction. First, droplets of a reactive solution of metal nitrate and glycine enter the tubular furnace, where they are preheated. Then, due to the rapid evaporation of water and a high concentration of reagents, hollow microspheres are formed from the dried nitrate–glycine mixture.[25] Secondly, exothermic decomposition reactions of precursors take place in each droplet (micro-combustors). These reactions lead to nuclei formation on the entire surface of the former droplets with their subsequent growth, coalescence, sintering and faceting, resulting from which a spherical framework (porous shell) is formed. Thus, one droplet forms a hollow metal oxide sphere with silver islands transforming into the metal separately compared to the formation of a shell. The fast surface diffusion and poor wetting of SPION with silver result in regional phase separation, which is quite typical for PPs. It is also evident from Figures 2(*d*)–(*l*) and 3(*f*) that the initial composition of the precursor solution makes it possible to control either the size of the silver regions or

[§] STEM images and mapping were performed on a Jeol JEM 2100F instrument. XRD was measured using a Rigaku D/MAX 2500 diffractometer with a rotating copper anode in the range of 10–80° in 0.02° increments. The Scherrer formula was used to determine the size of crystalline blocks. The reference data were taken from the PDF2 database. Magnetic measurements were carried out using a Faraday balance in the range from –18 000 to 18 000 Oe.

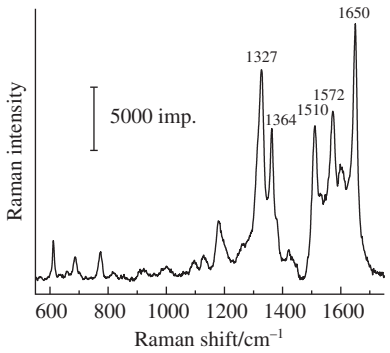

Figure 4 Typical SERS spectrum of the Rhodamine 6G dye at concentartion of 10^{-8} M measured using the PPs samples shown in Figure 2.

the amount of the SPION component in the PP shell, providing an overall attainable balance between the plasmonic and magnetic properties of PPs.

The practical application of the prepared PPs can be associated with SERS measurements and, possibly, with the capture of the analyte, its magnetic separation and optical analysis of target samples; the data in Figure 4¶ indicate at least that PPs can provide a significant Raman enhancement. The standard dye Rhodamine 6G, commonly used at nanomolar concentrations for testing SERS materials, exhibits all signals as bright and sharp peaks. There are no additional spectral features of organic residues from organic 'fuel' and nitrate groups, provided that SERS remains a susceptible tool for detecting such contaminants.[8] At the same time, the PPs themselves did not exhibit a Raman signal compared to some other problematic prehistories[8] due to the preparation at high temperatures and the removal of any organic impurities. Another thinkable advantage of such PPs is the presence of numerous 'hot spots' formed by closely spaced silver regions (see Figure 2), as they are generally known to provide more significant enhancement.[7,8]

Thus, we have reported a novel modification of solution combustion synthesis as a suitable and straightforward method for producing promising new PPs. We believe that the developed method is universal and allows one to synthesize various PPs merely by varying the synthesis parameters and processing conditions.

This work was performed according to the Development program 'The future of the planet and global environmental change' of the Interdisciplinary Scientific and Educational School of M. V. Lomonosov Moscow State University and the leading scientific school program (grant no. NSh 2726.2020.3). The SEM measurements were performed in part using the equipment of the Program of Research and Development of Moscow State University and Joint Research Centre for Physical Methods of Research of N. S. Kurnakov Institute of General and Inorganic Chemistry, Russian Academy of Sciences. Authors thank A. S. Sarycheva, A. E. Barantchikov, V. K. Ivanov, A. V Egorov and A. V. Savilov for their help. AAS thanks the Russian Science Foundation (grant no. 20-73-00257) for support.

¶ RS and SERS spectra were measured with a Renishaw InViva Raman microscope at 10% of 20 mW nominal laser power and 514 or 633 nm wavelength. The accumulation of spectra using a 50× long-focus lens was typically 10–60 s. Silicon wafers were used as a reference to adjust the peak position. Rhodamine 6G shows strong luminescence without PPs at concentrations above 10^{-8} M and contributes to the background signal only at concentrations below this threshold.

References

1 S. Ravaine and E. Duguet, *Curr. Opin. Colloid Interface Sci.*, 2017, **30**, 45.
2 F. Li, D. P. Josephson and A. Stein, *Angew. Chem., Int. Ed.*, 2011, **50**, 360.
3 C. Kaewsaneha, P. Tangboriboonrat, D. Polpanich, M. Eissa and A. Elaissari, *ACS Appl. Mater. Interfaces*, 2013, **5**, 1857.
4 X.-Y. Dong, Z.-W. Gao, K.-F. Yang, W.-Q. Zhang and L.-W. Xu, *Catal. Sci. Technol.*, 2015, **5**, 2554.
5 C. Zhan, X.-J. Chen, J. Yi, J.-F. Li, D.-Y. Wu and Z.-Q. Tian, *Nat. Rev. Chem.*, 2018, **2**, 216.
6 E. A. Goodilin, P. S. Weiss and Y. Gogotsi, *ACS Nano*, 2019, **13**, 10879.
7 O. E. Eremina, A. A. Semenova, E. A. Sergeeva, N. A. Brazhe, G. V. Maksimov, T. N. Shekhovtsova, E. A. Goodilin and I. A. Veselova, *Russ. Chem. Rev.*, 2018, **87**, 741.
8 A. A. Semenova, A. P. Semenov, E. A. Gudilina, G. T. Sinyukova, N. A. Brazhe, G. V. Maksimov and E. A. Goodilin, *Mendeleev Commun.*, 2016, **26**, 177.
9 A. S. Sarycheva, A. A. Semenova, E. Y. Parshina, N. A. Brazhe, A. Yu. Polyakov, A. Y. Kozmenkova, A. V. Grigorieva, G. V. Maksimov and E. A. Goodilin, *Mater. Lett.*, 2014, **121**, 66.
10 A. A. Semenova, N. A. Brazhe, E. Y. Parshina, V. K. Ivanov, G. V. Maksimov and E. A. Goodilin, *Plasmonics*, 2014, **9**, 227.
11 E. Yu. Parshina, A. S. Sarycheva, A. I. Yusipovich, N. A. Brazhe, E. A. Goodilin and G. V. Maksimov, *Laser Phys. Lett.*, 2013, **10**, 075607.
12 N. A. Brazhe, E. Y. Parshina, V. V. Khabatova, A. A. Semenova, A. R. Brazhe, A. I. Yusipovich, A. S. Sarycheva, A. A. Churin, E. A. Goodilin, G. V. Maksimov and O. V. Sosnovtseva, *J. Raman Spectrosc.*, 2013, **44**, 686.
13 G. V. Trusov, A. B. Tarasov, E. A. Goodilin, A. S. Rogachev, S. I. Roslyakov, S. Rouvimov, K. B. Podbolotov and A. S. Mukasyan, *J. Phys. Chem. C*, 2016, **120**, 7165.
14 P. Roth, *Proc. Combust. Inst.*, 2007, **31**, 1773.
15 H. K. Kammler, L. Mädler and S. E. Pratsinis, *Chem. Eng. Technol.*, 2001, **24**, 583.
16 A. E. Sytschev and A. G. Merzhanov, *Russ. Chem. Rev.*, 2004, **73**, 147 (*Usp. Khim.*, 2004, **73**, 157).
17 S. T. Aruna and A. S. Mukasyan, *Curr. Opin. Solid State Mater. Sci.*, 2008, **12**, 44.
18 K. C. Patil, S. T. Aruna and T. Mimani, *Curr. Opin. Solid State Mater. Sci.*, 2002, **6**, 507.
19 A. S. Mukasyan, A. S. Rogachev and S. T. Aruna, *Adv. Powder Technol.*, 2015, **26**, 954.
20 A. S. Mukasyan and P. Dinka, *Int. J. Self-Propag. High-Temp. Synth.*, 2007, **16**, 23.
21 B. Buesser and S. E. Pratsinis, *Annu. Rev. Chem. Biomol. Eng.*, 2012, **3**, 103.
22 R. Strobel, A. Baiker and S. E. Pratsinis, *Adv. Powder Technol.*, 2006, **17**, 457.
23 H. S. Kang, Y. C. Kang, H. D. Park and Y. G. Shul, *Mater. Lett*., 2003, **57**, 1288.
24 V. S. Shabde, S. V. Emets, U. Mann, K. A. Hoo, N. N. Carlson and G. M. Gladysz, *Comput. Chem. Eng.*, 2005, **29**, 2420.
25 A. B. D. Nandiyanto and K. Okuyama, *Adv. Powder Technol.*, 2011, **22**, 1.

Received: 14th December 2020; Com. 20/6395